Research Article | Vol. 26, No. 26 | 24 Dec 2018 | OPTICS EXPRESS 34131
Optics EXPRESS

New spectral reduction algorithm for echelle spectrometer in laser-induced breakdown spectroscopy

MENG SHEN,[1] ZHONGQI HAO,[1,3] XIANGYOU LI,[1,*] CHANGMAO LI,[2] LIANBO GUO,[1] YUN TANG,[1] PING YANG,[1] XIAOYAN ZENG,[1] AND YONGFENG LU[1]

[1] *Wuhan National Laboratory for Optoelectronics (WNLO), Huazhong University of Science and Technology (HUST), Wuhan, Hubei 430074, China*
[2] *Science and Technology on Surface Physics and Chemistry Laboratory, Mianyang, Sichuan 621700, China*
[3] *hzq@hust.edu.cn*
[*] *xyli@hust.edu.cn*

Abstract: In this work, a new spectral reduction algorithm for the echelle spectrometer was proposed. Unlike conventional approaches, the key concept in this algorithm is to model the spectrogram rather the spectrometer, which makes the algorithm more adaptive to different designs. This algorithm also introduces a dynamic adjusting procedure for generating optimized spectra from laser-induced plasmas. This additional step improved the spectrum stability and absolute line intensity of the spectrum and yielded better quantification performance. Experimental results demonstrated that the quantification results of analyzing aluminum alloy samples were improved using this new algorithm.

1. Introduction

Laser-induced breakdown spectroscopy (LIBS) is a kind of atomic emission spectroscopy which using high energy laser beams as excitation source. Compared with other detection technologies, LIBS provides the ability of *in situ* and real-time spectral analysis for unpretreated samples. What's more, when the system is built with a broadband spectrometer, like an echelle spectrometer or multi-channel optical fiber spectrometer, it gets the ability to analyze multiple elements simultaneously. Owing to these advantages, researches on LIBS and its applications have witnessed rapid growth over the past few years, and it has been applied to various fields such as coal-fired power stations, environmental protection and metallurgical industry [1–4].

As a key component in LIBS instrument, the performance of a spectrograph has crucial influence on sensitivity and precision of LIBS. More precisely, the spectral coverage and resolution of a spectrograph are the two most important parameters for setting up a LIBS system. With a broader spectral coverage, the spectrograph could provide more information for further analysis, which is the foundation for techniques like Calibration-Free LIBS (CF-LIBS) and multivariate data analyzing [5–8]. Owing to the specially designed structure using high order diffraction and twofold dispersion, the echelle spectrograph can provide wide spectral coverage with high diffraction efficiency and spectral resolution in a compact size [9]. When coupled with an intensified charge-coupled device (ICCD) camera, this spectrometer can provide high time resolution for fast decay spectra like laser-induced plasma spectra. Therefore, these characters make the combination of an echelle spectrograph with ICCD detector an ideal tool for LIBS determining elements within complex matrices like iron or titanium samples *etc.*, and much research has been reported with this setup [10, 11].

Generally, the captured images (*i.e.* spectrograms) are hardly used for analysis directly, since

#344970 https://doi.org/10.1364/OE.26.034131
Journal © 2018 Received 5 Sep 2018; revised 6 Dec 2018; accepted 6 Dec 2018; published 17 Dec 2018

Optics EXPRESS

the relation between spectral wavelength and intensity is difficult to tell from the spectrograms. A data transformation algorithm is usually performed on each spectrogram to create a corresponding one-dimensional spectrum, and the algorithm is called spectral reduction algorithm. The algorithm for one-dimensional dispersing system can be as simple as a low-order polynomial. However, due to the nature of cross-dispersion and non-linearity of a prism, the reduction algorithm for echelle spectrograph is more complex. To improve the accuracy, generality and efficiency of the reduction algorithm is still an active area of research [12–14].

Due to the ambient temperature changing and mechanical vibration, the component state of spectrometer will vary during a time-consuming data acquisition process. Since the reduction model used in conventional algorithms is established with fixed parameters, the accuracy of these algorithms will get deteriorated over time. When these misinterpreted spectra are used for analyzing in LIBS, the measurement results will become unreliable or even incorrect. Unlike other spectroscopy analytical methods, which are generally be carried out in the laboratory, providing reliable spectra is an essential requirement while taking LIBS instruments into industrial applications. Although there are several available techniques solving this problem, like coupling a built-in calibration lamp to calibrate the spectrometer after detecting temperature change [15] or adjust system parameters of the spectrograph [13]. These methods all require a comprehensive knowledge about the echelle spectrograph, and some even require extra modification of the instrument with additional calibration lamp.

To solve the problems mentioned above, a self-correcting reduction algorithm was proposed. The principle of this algorithm was introduced in detail, and the stability and performance of LIBS analysis using this algorithm and the manufacture built-in algorithm were compared.

2. Theory and method

The basic idea behind our algorithm is modeling the spectrogram and using several known reference inputs (*i.e.* monochromatic light beams and corresponding coordinates) to dynamically adjust the model to its accurate state. To represent our idea clearly, in the following subsections, we firstly explain the basic principle of the echelle spectrometer so that the formulation of wavelength and pixel position can be given, and then give the details about how this algorithm is performed. Finally, the tuning process for generating the spectrums is described.

2.1. Principle of echelle spectrograph

As shown in Fig. 1, a simplified optical layout of typical echelle spectrograph is demonstrated. Firstly, the light beam is collimated by a slit and a collimating mirror. Next, this light is dispersed by an echelle grating and a dual-component prism. Finally, this two-pass dispersed light gets focused to a detector by a focusing mirror. Since there are no moving components in this design, the spectrograph can be more reliable and robust compared to other types of spectrographs.

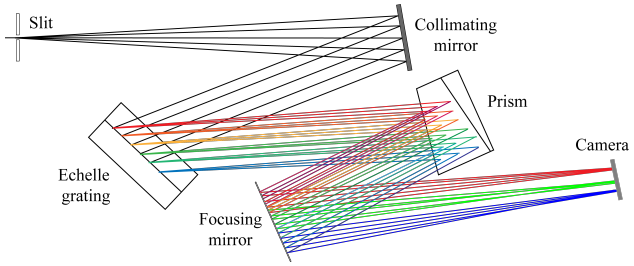

Fig. 1. Simplified optical layout of the echelle spectrograph, and correction lens used for reducing aberrations is omitted.

Optics EXPRESS

Under the assumption of an ideal condition and from the geometric aspect only, *i.e.*, without considering the optical aberration and the dispersion only comes from the prism and the echelle grating, a further simplified model could be given [16]. With this model, as shown in Fig. 2(a), the light gets dispersed by an echelle grating in the horizontal direction (parallel to X axis) firstly, and then gets further dispersed by prism in the vertical direction (parallel to Y axis). When this dispersed light gets focused on the detector, as illustrated in Fig. 2(b), a spectrogram (echellegram) is obtained. Owing to the non-linearity dispersion between different orders, these sloped lines are nonparallel to each other.

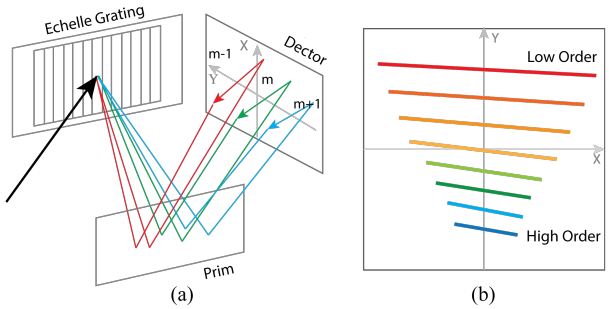

Fig. 2. Simplified light path of echelle spectrograph (a) and corresponding echellegram (b), light from same diffraction order is painted with same color.

In the horizontal direction, dispersion is caused by echelle grating solely, and can be expressed as grating Eq. (1). Where m is the order number, λ is the wavelength, a is the grating space, α is the fixed angle of incidence, and β_λ is then angle of diffraction of wavelength λ.

$$m\lambda = a * (\sin\alpha + \sin\beta_\lambda) \tag{1}$$

As indicated by the equation, with different diffraction order, one specified monochromatic light (λ is constant) will be dispersed toward several different angles, and at one specified diffraction angle (β_λ is constant) there will be several different wavelengths overlapped with each other.

Since the echelle grating is designed to operate at high diffraction orders (typical from 20 to 120) for achieving good efficiency within wide spectral range, the spectral overlapping between adjacent orders are much more severe than the traditional grating systems. To solve this problem, a secondary dispersion is introduced by using a prism to further disperse light in vertical direction.

In this perpendicular direction, dispersion caused by a prism can be expressed using Eq. (2). Where δ_λ is the dispersion angle, n_λ is the refractive index at given wavelength λ, and φ is the incidence angle, ϕ is the apex angle.

$$\delta_\lambda = \arcsin\{n_\lambda * \sin[\varphi - \arcsin(\frac{\sin\phi}{n_\lambda})]\} \tag{2}$$

Considering that each pixel's position value x is directly mapped to one particular echelle diffraction angle, and this mapping may be written as Eq. (3),

$$\beta_\lambda = F(x) \tag{3}$$

And doing a series expansion on the right part of Eq. (1), the relationship between x and λ can be further expressed using Eq. (4). Where p_i are constants of this polynomial function.

$$m\lambda = P(x) = \sum_{i=0}^{N} p_i x^i \tag{4}$$

Optics EXPRESS

Similarly, for the prism dispersion, like the above explanation for echelle dispersion, the relationship between y and λ can also be expressed in a polynomial Eq. (5). Where q_i are also constants.

$$\lambda = Q(y) = \sum_{i=0}^{M} q_i * y^i \tag{5}$$

With Eqs. (4) and (5), the relation of each pixel's position (x, y) and wavelength λ is fully established.

From these two equations, it is not hard to get the point that the relationship between wavelength and coordinates can be given by a series of constants. Therefore, how to calculate each pixel's wavelength is transformed to how to calculate the right value of $P = \{p_0, ..., p_N\}$ and $Q = \{q_0, ..., q_M\}$.

2.2. Method for building spectrogram model

Given the echelle model previously described, a spectrogram of two monochromatic lights (wavelength λ and λ' respectively) is illustrated in Fig. 3. For one specified monochromatic light, there will be several possible light spots along the X axis, and only some of these possible light spots can be seen owing to the dispersion efficiency. For the two lights with same diffraction angle, they are separated along the Y axis by prism dispersion.

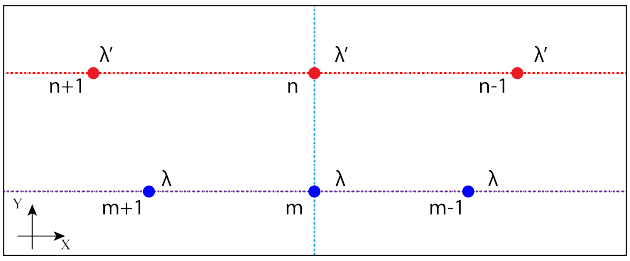

Fig. 3. Spectrogram of two monochromatic lights. Light spots with same wavelength are painted with same color.

For light spots with same wavelength, since the dispersion is solely caused by echelle grating, based on Eq. (4), the relationship between x and λ of two adjacent light spots can be given with Eqs. (6) and (7). Where x_r is the coordinate value of X axis of the right spot, and x_l is the coordinate value of X axis of the left spot.

$$m\lambda = P(x_r) = \sum_{i=0}^{N} p_i * x_r^i \tag{6}$$

$$(m-1)\lambda = P(x_l) = \sum_{i=0}^{N} p_i * x_l^i \tag{7}$$

For light spots from two different wavelengths at same diffraction angle, the dispersion is caused by the prism, based on Eq. (5), the relationship between y and λ of these two adjacent light spots can be given with Eqs. (8) and (9). Where y_n is the coordinate value of Y axis of at order n, and y_m is the coordinate value of Y axis of at order m.

$$\lambda_n = Q(y_n) = \sum_{i=0}^{M} q_i * y_n^i \tag{8}$$

Optics EXPRESS

$$\lambda_m = Q(y_m) = \sum_{i=0}^{M} q_i * y_m^i \tag{9}$$

From these Eqs. (6)-(9), if we take several known light spots' coordinates and their wavelengths, the specified values of P and Q for a given spectrometer will get calculated. And then the problem of how to calculate the values of P and Q is solved.

However, whether these calculated parameters can estimate other pixels' wavelength with high precision is still a problem, since this model is given under a lot of assumption and simplification. If taken consideration of (i) the difference of incidence angle in prism dispersion, and (ii) the distortion from aberration, the prerequisites for Eqs. (4) and (5) are not valid anymore. Therefore, Eqs. (6)-(9) are not strictly right and need adjustments [16, 17].

To compensate the difference between simplified model and the real one, Eqs. (4) and (5) are rewritten as Eqs. (10) and (11) respectively. Where $U(x, y)$ and $V(x, y)$ are the compensation parts with consideration of the coupling of x and y, and $U = \{u_{0,0}, ..., u_{J,J}\}$ $V = \{q_{0,0}, ..., q_{J,J}\}$ and two constants sets.

$$m\lambda = P(x) + U(x, y) = \sum_{i=0}^{N} p_i * x^i + \sum_{i=0}^{J}\sum_{j=0}^{J} u_{ij} * x^i * y^j \tag{10}$$

$$\lambda = Q(y) + V(x, y) = \sum_{i=0}^{M} q_i * y^i + \sum_{i=0}^{J}\sum_{j=0}^{J} v_{ij} * x^i * y^j \tag{11}$$

In order to calculate the values of P, Q, U and V, an iteration calculation process is used. In the initial iteration the compensate parts are omitted, and the order of Eqs. (4) and (5) is set no more than 2. After taking a set of known inputs (monochromatic light wavelength and corresponding pixels' coordinates), a rough spectrogram model can be established. In the next iteration, a new set of inputs will used for calculation, and the equations' order are increased for achieving better model fitting. By repeating this procedure, a spectrogram model with high precision is finally estimated.

2.3. Strategy for spectra reduction

After knowing each pixel's wavelength by modeling the spectrogram, the next step is to obtain the spectrum by calculating the single intensity at given wavelength. And Fig. 4 illustrated a commonly used strategy in conventional algorithms [18].

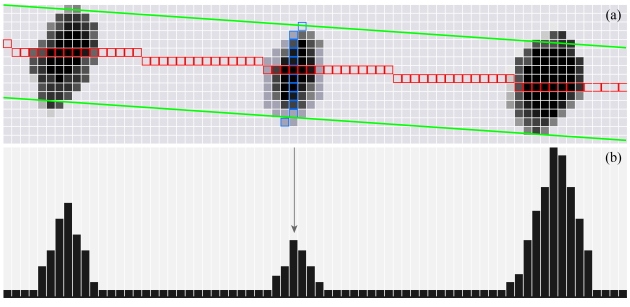

Fig. 4. A part of spectrogram within one order (a) and corresponding spectrum (b).

In this strategy, the spectral wavelength is a series of discrete values, which are the calculated pixels' wavelength. And these pixels are located along one specified order line, as illustrated by the pixels painted with red border in Fig. 4(a).

Optics EXPRESS

Since the input light beam is not an ideal point and existing the vertical dispersion caused by prism, the order lines have a thickness, as indicated by the two blue lines in Fig. 4(a). Therefore, the intensity of one given wavelength is the summation of adjacent pixels' intensity, which are perpendicular to the order line, as illustrated by these rectangles with blue border in Fig. 4(a). After calculating each intensity for these wavelengths at this order, a one-dimensional spectrum is finally deduced, as illustrated in Fig. 4(b).

However, if we take the quantification procedure used in LIBS into consideration, several drawbacks in this strategy will occur. (i) If the quantification model is established using the integral spectral intensity around a given wavelength, the spectral background will increase since this intensity will inevitably integrate several pixels which do not contain the signal of this spectral line. (ii) If the quantification model is established by using the maximum spectral intensity at given wavelength, the spectral intensity is more fragile to the deterioration of reduction accuracy since this intensity is built with only a subset of corresponding pixels.

Therefore, to avoid the drawbacks with this conventional strategy, we provided a different strategy for calculating the intensity by selecting the effective pixels around the central position of one given wavelength.

The judging function that used in this selection procedure can be formulated by Eqs. (12)-(14). Where $z_{x,y}$ represents the calculated judging factor at pixel position (x, y), $\widehat{x}$ and $\widehat{y}$ are the central pixel coordinate of the given spectral line, $i_{x,y}$ represents the pixel signal intensity at position (x, y), and c_1, c_2 are two constants.

$$z_{x,y} = F(\Delta i_{x,y}, \Delta r_{x,y}) \tag{12}$$

$$\Delta i_{x,y} = abs(i_{x,y} - i_{\widehat{x},\widehat{j}}) \tag{13}$$

$$\Delta r_{x,y} = c_1 * (x - \widehat{x})^2 + c_2 * (y - \widehat{y})^2 \tag{14}$$

Eq. 13 indicates the difference between the intensities at coordinate (x, y) and central $(\widehat{x}, \widehat{y})$. Eq. 14 indicates the distance between pixel (x, y) from central coordinate $(\widehat{x}, \widehat{y})$. Function F in Eq. 12 has the property that $z_{x,y} \propto \Delta i_{x,y}$ and $z_{x,y} \propto \Delta r_{x,y}$.

Therefore, for pixels whose judging factor exceeded certain threshold, *i.e.*, pixels who are either far from the central or do not contain a signal are omitted. Furthermore, since the pixels are dynamically selected, the spectral intensity can be more tolerant to spectrogram shifting caused by thermal changing and mechanical vibration.

3. Experimental

The schematic diagram of the experimental setup for LIBS is shown in Fig. 5. A Q-switched Nd:YAG laser (532 nm) operating at 10 Hz and pulse duration of 6 ns (Quantel Brilliant series) was used for sample ablation. The laser beam was focused onto the target at the normal incidence using a plano-convex lens (f=150 mm) and the focal point was fixed at 5 mm below the target surface. The target was mounted on a 3-axis translation stage for changing the analyzed locations and adjusting the target height. The plasma emission was collected by a light collector (Ocean Optics, 84-UV-25, wavelength range 200-2000 nm) and then coupled into a spectrometer through an optical fiber (Avantes Inc.). Both lasers and the ICCD camera were all synchronously controlled by a digital delay generator (Stanford Instrument, DG535). The acquired data were transported to computer for further analyzing.

A mercury lamp (Ocean Optics, HG-1) and krypton lamp (Ocean Optics, KR-1) were used for built spectrogram model and discuss the accuracy and stability of our approach. Six aluminum alloy samples were used in this study. The data was taken under optimized parameters with a laser

Optics EXPRESS

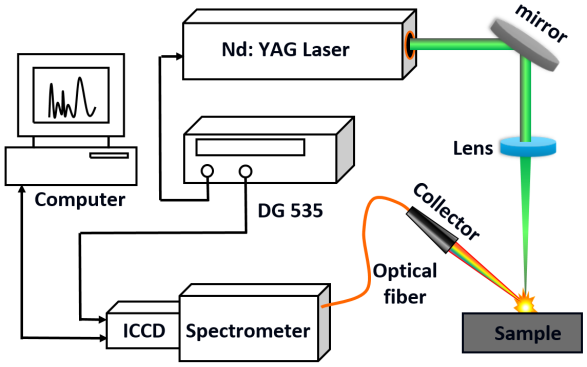

Fig. 5. The schematic diagram of experimental for LIBS.

energy of 50 mJ per pulse, an acquisition delay of 5 us, and a gate width of 5 us. Concentrations of these studied elements are listed in Table 1.

Table 1. Sample concentration (wt.%) of Si, Mn, Ni and Zn in aluminum samples

Sample	Si	Mn	Ni	Zn
E311	0.904	0.095	1.550	0.140
E312a	0.724	0.119	1.090	0.220
E313	1.220	0.239	2.020	0.334
E314	0.371	0.184	0.624	0.166
E315	1.530	0.287	0.153	0.367
E316	0.090	0.054	2.250	0.084

4. Results and discussion

4.1. Precision of the spectrogram model

To build the spectrogram model with high accuracy, there should be sufficient input values. Therefore, the mercury lamp whose emission spectrum fits the designed wavelength range (200 to 975 nm) of the spectrometer was used. A real spectrogram of the mercury lamp acquired by the echelle spectrometer in our instruments is shown in Fig. 6.

Since spectral intensity of 253.65 nm from mercury lamp is the strongest, when under a short exposure time, these firstly shown light spots are the most possible ones. Therefore, light spots in rectangle *A* are the dispersed lights with wavelength 253.65 nm, these are recognized.

Strategies used for identifying the wavelength in rectangles *B* and *C* are different from the former. Unlike the spectra with strongest intensity, these wavelengths are recognized based their spectrogram pattern. For mercury lamp spectrum, the only possible three adjacent spectra lines are 365.02, 365.48 and 366.33 nm, respectively. Therefore, the spectrogram pattern of three adjacent light spots in rectangle *B* must be these three wavelengths. For spots in rectangle *C*, their wavelength should be between 253.65 and 365.02 nm. Within this range, the only two adjacent spectra lines are 312.57 and 313.17 nm, respectively. Therefore, the wavelengths of two adjacent light spots in rectangle *B* are also recognized.

Optics EXPRESS

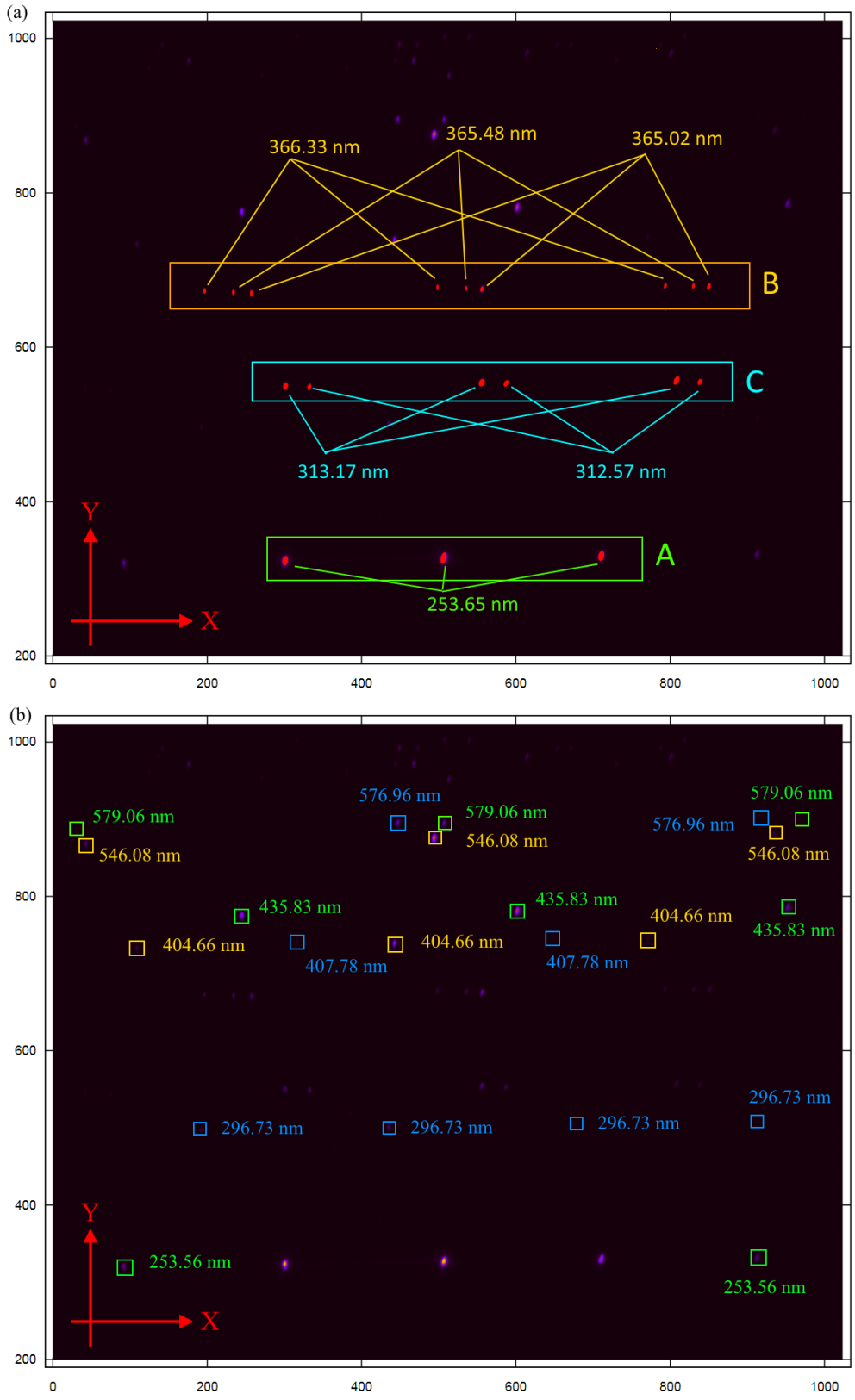

Fig. 6. Spectrograph of mercury lamp acquired by echelle spectrogram. Several easily identified light spots are marked with their wavelength and labeled by red dots in (a), other light spots identified by rough model are labeled by colored boxes in (b).

Optics EXPRESS

To identify other light spots which are not identified in previous procedure, these easily identified light spots are used as the basic inputs to build a rough spectrogram model. With this low precision model, and owing to the fact that the real coordinates should just near the calculated ones, the coordinates for other spectral lines are identified.

After identified all the light spots, and using these values as the inputs for the iteration calculation procedure described in Section 2.1, a spectrogram model with high precision is estimated. While using a krypton lamp as the validation group, the difference between the estimated coordinates and the real ones is typically less than 0.32 pixel. Therefore, the spectral precision that provided by our approach can fulfill the requirement in the real application.

4.2. Performance of the thermal stability

To investigate the thermal stability of the reduction algorithm, several spectrograms from mercury lamp were captured with same exposure time of 0.2 s but at a different room temperature, this changed from 21.4 to 24.2 °C.

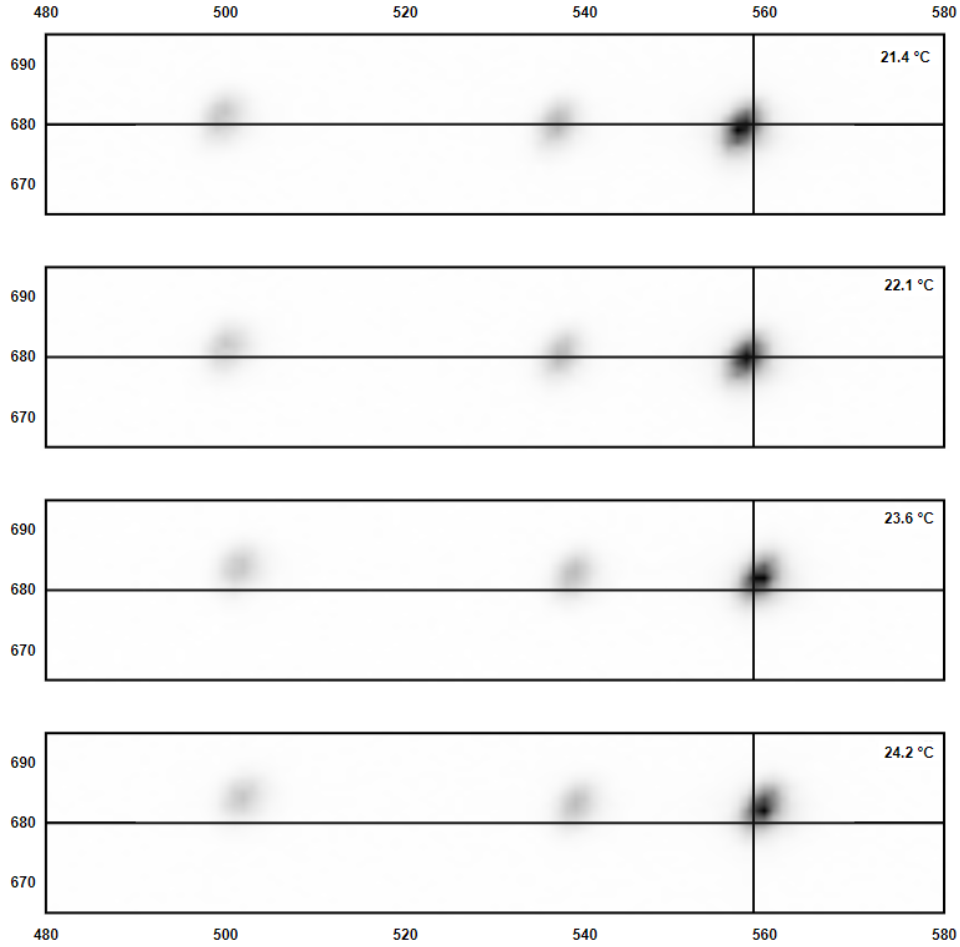

Fig. 7. Spectrogram shifting caused by thermal changing.

As illustrated in Fig. 7, we can see a clean spectrogram shifting process with the changing of room temperature. And, since the conventional algorithm (spectrums generated by the

Optics EXPRESS

manufacture build-in software) cannot compensate this variation, this shifting will cause severe intensity decline and wavelength shifting, as shown in Fig. 8(a).

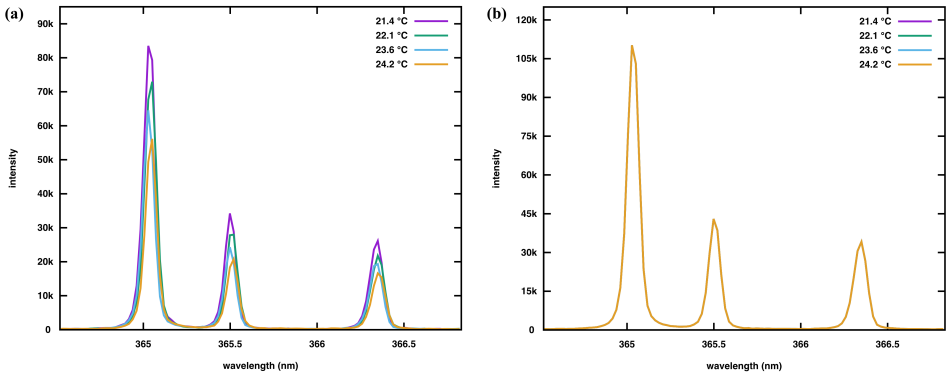

Fig. 8. Spectra comparison between two different algorithms after thermal changing. Intensity decreasing and wavelength drafting can be easily observed in (a), and since the spectra generated by the new algorithm got calibrated automatically, these lines are tightly overlapped in (b).

In contrast with the conventional approach, as illustrated in Fig. 8(b), contribute to the ability of compensating thermal drafting automatically in the new algorithm, the spectral wavelengths and intensities remain nearly constant after thermal changing. And, since the new algorithm can use more effective pixels by dynamically selecting, other then the conservative fixed size in conventional algorithm, the spectral intensities also improved.

4.3. *Performance of the algorithm in LIBS*

To investigate the impact on quantitative performance, *i.e.*, linearity coefficient (R^2), limit of detection (LoD), and root mean square error of cross-validation (RMSECV), seven aluminum alloy samples were used.

As shown in Table 2, for results from integration based spectral intensity calculation procedure owing to the ability of compensating thermal drafting and selecting effective pixels, results of R^2, LoD and RMSECV are all generally improved.

Table 2. Quantitative results at different wavelength

Analytical Line		Quantification Results †		
Element	λ (nm)	R^2	LoD (ppm)	RMSECV (ppm)
Si	288.16	0.8303 / 0.8742	77.69 / 41.74	95.01 / 76.31
Mn	403.31	0.9402 / 0.9704	47.69 / 11.15	38.22 / 12.31
	403.45	0.9366 / 0.9683	42.03 / 8.37	38.01 / 12.85
Ni	341.48	0.9153 / 0.9408	60.27 / 21.51	85.01 / 56.31
	352.45	0.9688 / 0.9821	47.02 / 18.18	31.01 / 16.63
Zn	334.50	0.9614 / 0.9868	51.69 / 21.39	26.16 / 14.75
	481.05	0.9178 / 0.9452	31.69 / 17.49	44.06 / 25.16

† Former results are from conventional algorithm, and the laters are from the new approach.

Optics EXPRESS

5. Conclusions

In this work, a new spectrogram reduction algorithm is proposed for a commercially purchased echelle spectrometer in LIBS. Compared with conventional spectral reduction algorithm, this algorithm does not rely on specified components parameters, which makes this algorithm more adaptive different optical designs and easier to performed. Furthermore, with introducing a dynamic adjusting procedure, the stability and absolute line intensity of spectra get improved, and the quantification results of R^2, LoD and RMSECV were improved by 3.1%, 60% and 45% respectively for tested samples. The results demonstrated that this algorithm does yield better quantification performance even under ambient changing condition. Therefore, we believe this algorithm will be a useful tool for LIBS in the industrial applications.

Funding

Major Scientific Instruments and Equipment Development Special Funds of China (2011YQ160017); National Natural Science Foundation of China (11874167).

References

1. J. Feng, Z. Wang, L. West, Z. Li, and W. Ni, "A pls model based on dominant factor for coal analysis using laser-induced breakdown spectroscopy," Anal. Bioanal. Chem. **400**, 3261–3271 (2011).
2. S. Yao, J. Xu, X. Dong, B. Zhang, J. Zheng, and J. Lu, "Optimization of laser-induced breakdown spectroscopy for coal powder analysis with different particle flow diameters," Spectrochimica Acta Part B: At. Spectrosc. **110**, 146–150 (2015).
3. X. Y. Yang, Z. Q. Hao, C. M. Li, J. M. Li, R. X. Yi, M. Shen, K. H. Li, L. B. Guo, X. Y. Li, Y. F. Lu, and X. Y. Zeng, "Sensitive determinations of cu, pb, cd, and cr elements in aqueous solutions using chemical replacement combined with surface-enhanced laser-induced breakdown spectroscopy," Opt. Express **24**, 13410–13417 (2016).
4. L. Sun, H. Yu, Z. Cong, Y. Xin, Y. Li, and L. Qi, "In situ analysis of steel melt by double-pulse laser-induced breakdown spectroscopy with a cassegrain telescope," Spectrochimica Acta Part B: At. Spectrosc. **112**, 40–48 (2015).
5. E. Tognoni, G. Cristoforetti, S. Legnaioli, and V. Palleschi, "Calibration-free laser-induced breakdown spectroscopy: State of the art," Spectrochimica Acta Part B: At. Spectrosc. **65**, 1–14 (2010).
6. B. Praher, V. Palleschi, R. Viskup, J. Heitz, and J. Pedarnig, "Calibration free laser-induced breakdown spectroscopy of oxide materials," Spectrochimica Acta Part B: At. Spectrosc. **65**, 671–679 (2010). A Selection of Papers Presented at the 5th Euro-Mediterranean Symposium on Laser Induced Breakdown Spectroscopy (EMSLIBS 2009).
7. S. M. Clegg, E. Sklute, M. D. Dyar, J. E. Barefield, and R. C. Wiens, "Multivariate analysis of remote laser-induced breakdown spectroscopy spectra using partial least squares, principal component analysis, and related techniques," Spectrochimica Acta Part B: At. Spectrosc. **64**, 79–88 (2009).
8. Z. Wang, J. Feng, L. Li, W. Ni, and Z. Li, "A non-linearized pls model based on multivariate dominant factor for laser-induced breakdown spectroscopy measurements," J. Anal. At. Spectrom. **26**, 2175–2182 (2011).
9. P. Boumans and J. Vrakking, "High-resolution spectroscopy using an echelle spectrometer with predisperser—I. Characteristics of the instrument and approach for measuring physical line widths in an inductively coupled plasma," Spectrochimica Acta Part B: At. Spectrosc. **39**, 1239–1260 (1984).
10. J. L. Wu, Y. Lu, Y. Li, K. Cheng, J. J. Guo, and R. E. Zheng, "Time resolved laser-induced breakdown spectroscopy for calcium concentration detection in water," Optoelectronics Lett. **7**, 65–68 (2011).
11. X. Mao, X. Zeng, S.-B. Wen, and R. E. Russo, "Time-resolved plasma properties for double pulsed laser-induced breakdown spectroscopy of silicon," Spectrochimica Acta Part B: At. Spectrosc. **60**, 960–967 (2005). Laser Induced Plasma Spectroscopy and Applications (LIBS 2004) Third International Conference.
12. L. Yin, Bayanheshig, J. Yang, Y. Lu, R. Zhang, C. Sun, and J. Cui, "High-accuracy spectral reduction algorithm for the echelle spectrometer," Appl. Opt. **55**, 3574–3581 (2016).
13. R. Zhang, Bayanheshig, X. Li, and J. Cui, "Establishment and correction of an echelle cross-prism spectrogram reduction model," Opt. Commun. **403**, 401–407 (2017).
14. R. Zhang, Bayanheshig, L. Yin, X. Li, J. Cui, J. Yang, and C. Sun, "Wavelength calibration model for prism-type echelle spectrometer byreversely solving prism's refractive index in real time," Appl. Opt. **55**, 4153–4158 (2016).
15. R. M. Bernstein, S. M. Burles, and J. X. Prochaska, "Data reduction with the MIKE spectrometer," Publ. Astron. Soc. Pac. **127**, 911 (2015).
16. A. A. Dantzler, "Echelle spectrograph software design aid," Appl. Opt. **24**, 4504–4508 (1985).
17. D. A. Sadler, D. Littlejohn, and C. V. Perkins, "Automatic wavelength calibration procedure for use with an optical spectrometer and array detector," J. Anal. At. Spectrom. **10**, 253–257 (1995).
18. A. Scheeline, C. A. Bye, D. L. Miller, S. W. Rynders, and R. C. Owen, "Design and characterization of an echelle spectrometer for fundamental and applied emission spectrochemical analysis," Appl. Spectrosc. **45**, 334–346 (1991).